

# Large- $N$ limit of $O(N)^3$ -invariant general sextic tensor model

G. Bardy<sup>1</sup>, T. Krajewski<sup>2</sup>, T. Muller<sup>3</sup>, and A. Tanasa<sup>1,4</sup>

<sup>1</sup>*Univ. Bordeaux, LaBRI CNRS UMR 5800, Talence, France*

<sup>2</sup>*Aix Marseille Univ, Université de Toulon, CNRS, CPT, Marseille, France*

<sup>3</sup>*Univ. Sorbonne Paris Nord, LIPN UMR CNRS 7030, Villetaneuse, France*

<sup>4</sup>*DFT, H. Hulubei Nat. Inst. Phys. Nucl. Engineering, Magurele, Magurele, Romania*

November 6, 2025

## Abstract

We study a sextic tensor model where the interaction terms are given by all  $O(N)^3$ -invariant bubbles. The class of invariants studied here is thus a larger one than the class of the  $U(N)^3$ -invariant sextic tensor model. We implement the large  $N$  limit mechanism for our model and we explicitly identify the dominant graphs in the  $1/N$  expansion. This class of dominant graphs contains tadpole graphs, melonic graphs but also new types of tensor graphs. Our analysis adapts the tensorial intermediate field method, previously applied only to the prismatic interaction, to all connected sextic interactions except the wheel interaction, which we treat separately using a cycle analysis.

## 1. Introduction

The large- $N$  limit [1] is an important tool in quantum field theory. By extending the number of degrees of freedom  $N \rightarrow \infty$  and suitably rescaling the coupling constants by powers of  $N$ , one reorganizes the perturbative expansion in powers of  $1/N$ , often allowing for controlled, analytic computations in otherwise intractable systems.

We know so far three type of QFT models where one can successfully implements the large  $N$  limit mechanism: vector, matrix, and tensor models. In vector models [2], cactus diagrams dominate the  $1/N$  expansion, rendering the theory essentially solvable. Such models are central to the study of critical phenomena. Matrix models generate ribbon graphs (or combinatorial maps) *via* perturbative expansion, their large- $N$  limit is dominated by planar diagrams [3–6]. The sum over ribbon graphs, organized by the genus, corresponds to a sum over discretized two-dimensional surfaces thus providing a natural framework for random geometry in  $d = 2$  [7,8] and for two-dimensional quantum gravity [9–11].

Tensor models were originally introduced as descriptions of random geometries in higher dimension [12,13]. Their large- $N$  behavior was discovered much later, see the books [14,15]. It is governed by melonic diagrams [16], which form a subset of planar diagrams. The melonic limit is, from this diagrammatic point of view, simpler than the planar one yet richer than the cactus one, and thus captures nontrivial dynamics.

The same melonic large- $N$  limit appears in the celebrated Sachdev–Ye–Kitaev (SYK) model, initially introduced for spin glasses [17]. The SYK model describes  $N$  Majorana fermions with random interactions, averaged over disorder, and has attracted a wide interest as a toy model for holography [18]. Tensor models provide a disorder-free reformulation of the SYK model [19–21], motivating the development of tensor field theories in  $d > 0$  [22–25].

The  $1/N$  expansion of tensor models is controlled by the degree [16, 26]. Understanding the large- $N$  limit of a specific model is a prerequisite both for studying it as a field theory and for combinatorial analyses such as the double scaling limit [27, 28]. This paper addresses this question for the  $O(N)^3$ -invariant sextic tensor model.

Recall that  $O(N)^3$ -invariant tensor models were first introduced in [29], where the large- $N$  limit of the quartic model was implemented. Field-theoretic studies of this model followed in [22, 24]. In the sextic case, the large- $N$  limit of the  $U(N)^3$  model was derived in [30] (see also [31, 32]). Its set of interactions is a subset of those of the  $O(N)^3$ -invariant model that we study in this paper. A renormalization group study for the  $U(N)^3$ -invariant model was then performed in [33].

The so-called prismatic model [23] was also solved at large  $N$ , though with scalings which favor a particular sextic interaction, the prismatic one (this is motivated by the renormalization group study performed in that paper). A sextic model with a reduced set of  $O(N)^3$ -invariant interaction was also studied in [34]. More recently, perturbative field-theoretic computations on the full  $O(N)^3$  sextic model, including a Yukawa interaction, were carried out in [35].

Nevertheless, the large- $N$  limit of the sextic model taking into consideration all  $O(N)^3$  invariant interactions with optimal scalings has remained unknown. In this paper, we implement this large  $N$  limit and we explicitly exhibit the dominant graphs.

The class of dominant graphs we find is significantly larger than the class of graphs found for the prismatic model [23] or the one found for the  $U(N)^3$  invariant model. This is a direct consequence of the fact that the class of  $O(N)^3$  invariant interaction is larger than the class of  $U(N)^3$  invariant interactions.

Let us emphasize that this class of dominant graphs we find here contains tadpole graphs, the celebrated melonic graphs but also new types of graphs.

To identify these dominant Feynman graphs, we employ the intermediate field method [36, 37], which is adapted in a non-trivial way to tensorial interactions, see [28, 38, 39]. In order to obtain the class of dominant graphs of our model, we prove that the intermediate field method decomposes most of the sextic tensor interactions into quartic ones and it reduces, from a diagrammatic point of view, the analysis of our general model to a minimal set of interactions: the tetrahedron and the wheel  $K_{3,3}$ .

The paper is organized as follows. Section 2 introduces the  $O(N)^3$ -invariant sextic model, which has 8 invariant bubbles. Moreover, we define the notion of  $l$ -cycles in Feynman graphs. Section 3 exhibits the intermediate field method for all connected sextic interactions, except the wheel interaction. We also prove in section 4 that, from a diagrammatic point of view, the general sextic model is equivalent to a reduced model containing only wheel and tetrahedron interaction. Section 4 then analyzes this reduced model. We bound the number of cycles in dominant graphs, and we show that no fundamental dominant graph can contain a wheel interaction and another sextic interaction. Section 5 then gives the lists of dominant graphs of our general model. We also explicitly exhibit the 2-point and 6-point insertions which conserve the degree. The last section is dedicated to the conclusions of the paper.

## 2. The general sextic model

### 2.1. The action of the model

Random tensor models are 0–dimensional field theoretical models, where the fields are rank  $r$  tensors  $T^{i_1 i_2 \dots i_r}$ , with  $i_1, \dots, i_r \in \{1, \dots, N\}$ .

One usually imposes invariance of tensor models under the action of  $r$  copies of a certain group  $G$  (see again the books [14, 15]). The tensor transforms as

$$T_{a_1 a_2 \dots a_r} \rightarrow R_{a_1 b_1}^{(1)} R_{a_2 b_2}^{(2)} \dots R_{a_r b_r}^{(r)} T_{b_1 b_2 \dots b_r}, \quad (1)$$

where the  $R^{(k)}$  are in the fundamental representation of  $G$ . The action of the given model has to be invariant under the transformation (1). The group  $G$  can thus be  $O(N)$  (see [23, 25, 29]),  $U(N)$  [33, 40] or  $Sp(2N)$  [41]. Note that the duality between  $O(N)$  and  $Sp(2N)$  invariance [42], known for vector and matrix models [43], also holds in the case of random tensors (see [44–47]).

The partition function of such a model writes

$$\mathcal{Z} = \int [dT] e^{-N^{r/2} S[T]}. \quad (2)$$

where the action writes:

$$S[T] = S_0[T] + S_{\text{int}}[T].$$

The free part writes:

$$S_0[T] = \frac{1}{2} T_{i_1, \dots, i_r} T_{i_1, \dots, i_r}.$$

The interacting part of the action is a sum over the so-called bubbles (which are the interacting terms)

$$S_{\text{int}}[T] = \sum_b \frac{g_b}{N^{\rho(b)}} I_b(T), \quad (3)$$

where  $I_b(T)$  is invariant under the action of  $G^r$  and  $\rho$  is an appropriate scaling of the bubble.

The partition function for the general  $O(N)^3$ -invariant sextic model writes

$$\mathcal{Z} = \int [dT] e^{-N^{3/2} S[T]}, \quad (4)$$

with

$$S[T] = \frac{1}{2} T_{i_1 i_2 i_3} T_{i_1 i_2 i_3} + \sum_{b=1}^8 \frac{g_b N^{-\rho(b)}}{6} I_b(T), \quad (5)$$

where  $I_b(T)$  denotes the  $b$ -th invariant bubble and  $\rho(b)$  its scaling.

The sextic bubbles have the general form

$$I_b(T) = \delta_{\mathbf{a} \mathbf{b} \mathbf{c} \mathbf{d} \mathbf{e} \mathbf{f}}^{(b)} T_{\mathbf{a}} T_{\mathbf{b}} T_{\mathbf{c}} T_{\mathbf{d}} T_{\mathbf{e}} T_{\mathbf{f}}, \quad (6)$$

where  $\mathbf{a} = (a_1 a_2 a_3)$  and  $\delta_{\mathbf{a} \mathbf{b}} = \prod_{i=1}^3 \delta_{a_i b_i}$ . The indices contractions, symmetrized under color permu-

tations, but not under external indices, are

$$\begin{aligned}
\delta_{\mathbf{abcdef}}^{(1)} &= \delta_{a_1 b_1} \delta_{b_2 c_2} \delta_{c_1 d_1} \delta_{d_2 e_2} \delta_{e_1 f_1} \delta_{f_2 a_2} \delta_{a_3 e_3} \delta_{b_3 d_3} \delta_{f_3 c_3}, \\
\delta_{\mathbf{abcdef}}^{(2)} &= \delta_{a_1 b_1} \delta_{b_2 c_2} \delta_{c_1 d_1} \delta_{d_2 e_2} \delta_{e_1 f_1} \delta_{a_2 f_2} \delta_{a_3 d_3} \delta_{b_3 e_3} \delta_{c_3 f_3}, \\
\delta_{\mathbf{abcdef}}^{(3)} &= \frac{1}{3} (\delta_{a_1 f_1} \delta_{a_2 b_2} \delta_{a_3 b_3} \delta_{b_1 c_1} \delta_{c_2 f_2} \delta_{c_3 d_3} \delta_{e_3 f_3} \delta_{d_1 e_1} \delta_{d_2 e_2} + (1 \leftrightarrow 2) + (1 \leftrightarrow 3)), \\
\delta_{\mathbf{abcdef}}^{(4)} &= \frac{1}{3} \sum_{i=1}^3 \delta_{a_i b_i} \delta_{c_i d_i} \delta_{e_i f_i} \prod_{j \neq i} \delta_{b_j c_j} \delta_{d_j e_j} \delta_{a_j f_j}, \\
\delta_{\mathbf{abcdef}}^{(5)} &= \frac{1}{3} (\delta_{a_1 f_1} \delta_{a_2 b_2} \delta_{a_3 b_3} \delta_{b_1 c_1} \delta_{c_2 e_2} \delta_{c_3 d_3} \delta_{d_1 e_1} \delta_{e_3 f_3} \delta_{d_2 e_2} + (1 \leftrightarrow 2) + (1 \leftrightarrow 3)), \\
\delta_{\mathbf{abcdef}}^{(6)} &= \delta_{a_1 b_1} \delta_{a_2 c_2} \delta_{a_3 d_3} \delta_{b_2 d_2} \delta_{b_3 c_3} \delta_{c_1 d_1} \delta_{\mathbf{ef}}, \\
\delta_{\mathbf{abcdef}}^{(7)} &= \frac{1}{3} (\delta_{a_1 b_1} \delta_{a_2 b_2} \delta_{b_3 c_3} \delta_{c_1 d_1} \delta_{c_2 d_2} \delta_{a_3 d_3} + (1 \leftrightarrow 2) + (1 \leftrightarrow 3)) \delta_{\mathbf{fe}}, \\
\delta_{\mathbf{abcdef}}^{(8)} &= \delta_{\mathbf{ab}} \delta_{\mathbf{cd}} \delta_{\mathbf{ef}}.
\end{aligned} \tag{7}$$

The interaction terms are represented on Fig. 1. Note that we call  $I_1$  the prismatic interaction and  $I_2$  the wheel interaction.

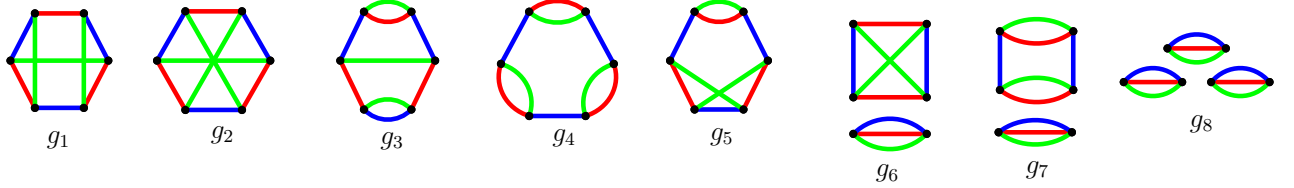


Figure 1: The  $O(N)^3$ -invariant sextic interactions. Color permutations are implicit.

In [23] the scalings were chosen to be

$$\rho_1 = 0, \quad \rho_2 = \rho_4 = \rho_6 = \rho_7 = 2, \quad \rho_3 = \rho_5 = 1, \quad \rho_8 = 4. \tag{8}$$

As already mentioned in the introduction, this choice of scaling was made in order to favor the prismatic interaction, because it is for this interaction that a thorough RG flow analysis was performed. However, we chose here a different set of scalings, which, following [29], is an optimal one, in the sense that all interactions can contribute in the large  $N$  limit. These scalings are

$$\rho(b) = \frac{1}{2} \sum_l \delta_l^{(b)}, \tag{9}$$

where  $\delta_l^{(b)} = |J_l^{(b)}| - 1$ , and  $|J_l^{(b)}|$  is the number of connected components of the  $l$ -th jacket of the bubble  $b$ , which is obtained by removing all the edges of color  $l$  in the bubble  $b$  [29].

For each sextic bubble we compute  $\rho(b)$  explicitly, obtaining the scalings shown in Fig. 39 (see Appendix A). One finds:

$$\rho_1 = \rho_2 = 0, \quad \rho_3 = \rho_4 = 1, \quad \rho_5 = \frac{1}{2}, \quad \rho_6 = \frac{3}{2}, \quad \rho_7 = 2, \quad \rho_8 = 3. \tag{10}$$

Note that, for the  $U(N)^3$ -invariant interactions  $I_2, I_3, I_4, I_7, I_8$ , our choice of scalings is the same as the one of [33]. Recall that the  $1/N$  expansion of tensor models is controlled by the degree of the graphs. By definition, the dominant graphs in the large  $N$  limit have vanishing degree [16]. The degree of a graph  $\mathcal{G}$  in this model is (see again [29] for the general formula)

$$\omega(\mathcal{G}) = 3 + \sum_{b \in V(\mathcal{G})} (3 + \rho(b)) - F(\mathcal{G}), \quad (11)$$

where  $V(\mathcal{G})$  is the set of interactions of the graph and  $F(\mathcal{G})$  is the number of faces of the graph.

## 2.2. Inequivalent cycles

The analysis of the  $O(N)^3$ -invariant sextic model requires a careful study of cycles in Feynman graphs. We collect here some useful definitions and results, following the presentation in [34].

A *cycle of length  $l$* , or  *$l$ -cycle*, is a set of edges visiting  $l$  distinct bubbles,

$$\mathcal{C}_l = \langle (V'_1, V_2), (V'_2, V_3), \dots, (V'_{l-1}, V_l), (V'_l, V_1) \rangle, \quad (12)$$

where  $V_i \neq V'_i$  are vertices in the  $i$ -th bubble graph (not vertices of the full Feynman graph).

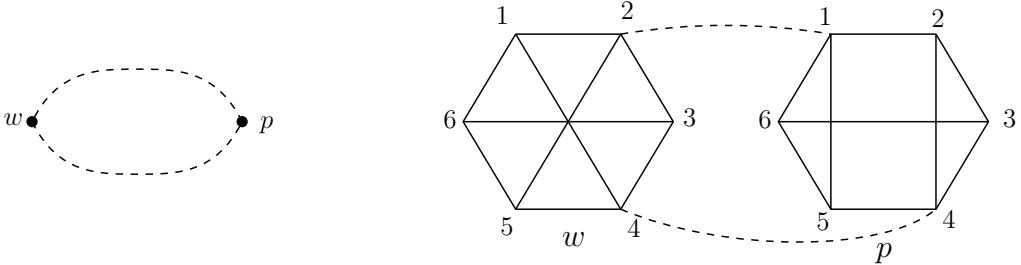


Figure 2: Example of a 2-cycle visiting a wheel and a prism in the Feynman (left) and bubble (right) representation,  $\mathcal{C}_2 = \langle (w_2, p_1), (p_4, w_4) \rangle$ .

Let us note that a cycle is not necessarily a closed loop in the bubble representation (see Fig. 2). When considering Feynman graphs where the internal structure of bubbles is not taken into consideration, the notion above boils down to the standard notion of a cycle in graph theory.

For a configuration of  $l$  bubbles, let  $z_i$  denote the number of vertices in the  $i$ -th bubble. The total number of  $l$ -cycles is then  $N_{\mathcal{C}_l} = \prod_{i=1}^l z_i(z_i - 1)$ . For example, in the sextic model there are 900 distinct 2-cycles.

Many of these cycles are equivalent under the symmetry group of the bubbles. Each bubble is invariant under two types of transformations: color permutations and automorphisms of the bubble. This defines a symmetry group  $\mathcal{S}_{\mathcal{G}}$ , acting as permutations on the vertex set of the full graph  $\mathcal{G}$ .

Two  $l$ -cycles  $\mathcal{C}_l$  and  $\mathcal{C}'_l$  are *equivalent* if there exists  $\sigma \in \mathcal{S}_{\mathcal{G}}$  such that  $\mathcal{C}_l = \sigma \cdot \mathcal{C}'_l$ . To identify inequivalent cycles under  $\mathcal{S}_{\mathcal{G}}$  we use the following procedure:

- Decompose the set of possible values of  $V'_1$ , i.e.  $\{1_1, 2_1, \dots, z_1\}$ , into distinct orbits under  $\mathcal{S}_{\mathcal{G}}$ :

$$\{1_1, 2_1, \dots, z_1\} = \bigsqcup_{\bar{V}'_1} \text{Orb}_{\mathcal{S}_{\mathcal{G}}}(\bar{V}'_1), \quad (13)$$

where  $\bar{V}'_1$  are orbit representatives.

- For each representative  $\bar{V}'_1$ , compute the stabilizer subgroup  $\text{Stab}_{\mathcal{S}_{\mathcal{G}}}(\bar{V}'_1) \subset \mathcal{S}_{\mathcal{G}}$  that leaves  $\bar{V}'_1$  fixed.
- Decompose the possible values of  $V_2$  into orbits under  $\text{Stab}_{\mathcal{S}_{\mathcal{G}}}(\bar{V}'_1)$ , and proceed iteratively. More generally, to fix  $\bar{V}_k$ , choose a representative of each orbit of  $\{1_k, 2_k, \dots, z_k\}$  under the stabilizer group  $\text{Stab}_{\mathcal{S}_{\mathcal{G}}}(\bar{V}'_1, \bar{V}_2, \dots, \bar{V}'_{k-1})$ .

This iterative decomposition provides the complete set of inequivalent  $l$ -cycles, modulo color permutations and bubble automorphisms. This dramatically reduces the number of cycles to be studied.

### 3. Intermediate field method for sextic interactions

As already mentioned in the introduction, the intermediate field method extends to tensorial interactions. This was already implemented for quartic interactions in [39]. Moreover, this method was also successfully applied to the prismatic interaction in [23, 28]. In this section we generalize the implementation of this method to the connected sextic interactions, except the wheel interaction. For this purpose, we use either a real intermediate tensor field or a complex intermediate tensor field.

#### 3.1. Real intermediate field

One rewrites the  $I_1$  interaction in the following way:

$$\exp \left[ -\frac{g_1 N^{3/2}}{6} I_1(T) \right] = \int [d\chi^{(1)}] \exp \left[ -N^{3/2} \left( \frac{1}{2} \chi_{ijk}^{(1)} \chi_{ijk}^{(1)} + i \sqrt{\frac{g_1}{3}} \hat{I}_T(T, \chi) \right) \right], \quad (14)$$

where

$$\hat{I}_T(T, \chi^{(1)}) = T_{a_1 b_1 c_1} T_{a_1 b_2 c_2} T_{a_2 b_1 c_2} \chi_{a_2 b_2 c_1}^{(1)} \quad (15)$$

is a tetrahedric bubble represented on Fig. 3, and  $\chi^{(1)}$  is the intermediate field, here a rank 3 tensor field.

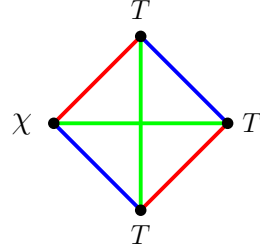


Figure 3: Tetrahedric term  $\hat{I}_T(T, \chi)$  with an intermediate field.

Therefore, a prismatic interaction can be decomposed in two tetrahedric interactions connected by an intermediate field  $\chi_{abc}^{(1)}$ , see Fig. 4.

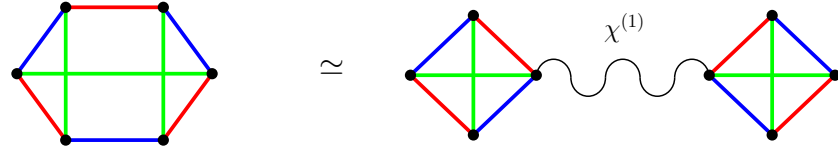


Figure 4: Decomposition of the prismatic interaction using a real intermediate field  $\chi_{abc}^{(1)}$ .

In an analogous way, the interaction  $I_4(T)$  can also be decomposed using a real intermediate field. The invariant is

$$I_4(T) = \frac{1}{3} (I_4^{(a)}(T) + I_4^{(b)}(T) + I_4^{(c)}(T)), \quad (16)$$

where

$$I_4^{(a)}(T) = T_{ab_1 c_1} T_{a_1 b c} T_{a_1 b_1 c_1} T_{ab_2 c_2} T_{a_2 b c} T_{a_2 b_2 c_2}, \quad (17)$$

and the other terms are obtained by the color permutations  $(a \leftrightarrow b)$  and  $(a \leftrightarrow c)$ . Each of these bubbles can be split as above, using the real intermediate field method. For example,  $I_4^{(a)}(T)$  can be

expressed as  $J_{abc}^{(a)} J_{abc}^{(a)}$  where  $J_{abc}^{(a)} = T_{ab_1 c_1} T_{a_1 b c} T_{a_1 b_1 c_1}$ .

The intermediate field is, in this case,  $\chi_{abc}^{(4,a)}$ . The resulting term in the path integral is:

$$\exp \left[ -\frac{g_4 N^{3/2-1}}{6} I_4^{(a)}(T) \right] = \int [d\chi^{(4,a)}] \exp \left[ -N^{3/2} \left( \frac{1}{2} \chi_{ijk}^{(4,a)} \chi_{ijk}^{(4,a)} + \frac{i}{N^{1/2}} \sqrt{\frac{g_4}{3}} \hat{I}_P^{(a)}(T, \chi) \right) \right], \quad (18)$$

where  $I_P^{(a)}(T, \chi) = T_{ab_1c_1} T_{a_1bc} T_{a_1b_1c_1} \chi_{abc}^{(4,a)}$  is a pillow bubble, represented on Fig. 5.

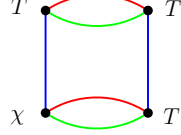


Figure 5: Pillow term  $\hat{I}_P^{(a)}(T, \chi)$  with an intermediate field.

This gives the decomposition for the  $I_4(T)$  interaction, as two pillows of the same color connected by a real intermediate field  $\chi_{abc}^{(4,a)}$ , see Fig. 6.

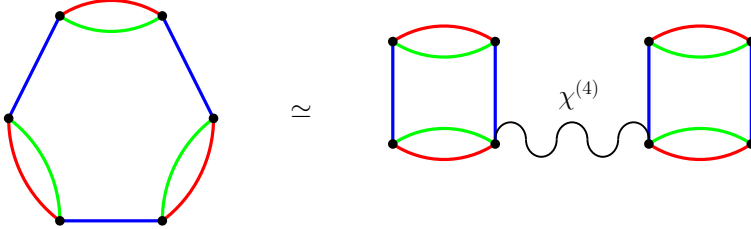


Figure 6: Decomposition of  $I_4(T)$  by an intermediate field.

### 3.2. Complex intermediate field

The mechanism described in the previous subsection cannot be directly applied for the  $I_3$  and  $I_5$  interaction terms of the model studied here. Nevertheless, for these interaction terms, we can adapt the previous intermediate field method using a complex intermediate field.

For these interactions, we define a complex intermediate field  $\chi$  and its complex conjugate  $\bar{\chi}$ :

$$\chi_{abc} = \frac{1}{\sqrt{2}} (\psi_{abc} + i\phi_{abc}), \quad \bar{\chi}_{abc} = \frac{1}{\sqrt{2}} (\psi_{abc} - i\phi_{abc}). \quad (19)$$

The  $I_5(T)$  bubble is thus decomposed as such:

$$\exp \left[ -\frac{g_5 N^{\frac{3}{2}-\frac{1}{2}}}{6} I_5(T) \right] = \int [d\chi^{(5)}] [d\bar{\chi}^{(5)}] \exp \left[ -N^{3/2} (\chi_{abc}^{(5)} \bar{\chi}_{abc}^{(5)} + i \sqrt{\frac{g_5}{6}} \hat{I}_T(T, \chi) + i N^{-1/2} \sqrt{\frac{g_5}{6}} \hat{I}_P(T, \bar{\chi})) \right], \quad (20)$$

where  $\hat{I}_T(T, \chi)$  is defined in eq. (15) and  $\hat{I}_P(T, \bar{\chi})$  is a pillow bubble.

Thus, the  $I_5$  interaction is split into a tetrahedron and a pillow interaction. This splitting is shown on Fig. 7.

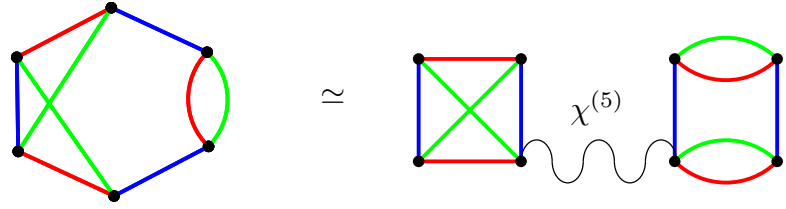


Figure 7: Intermediate field method for the  $I_5$  sextic interaction.

For the  $I_3(T)$  interaction, a normalization over color permutation is again necessary. One has

$$I_3(T) = \frac{1}{3}(I_3^{(a)}(T) + I_3^{(b)}(T) + I_3^{(c)}(T)), \quad (21)$$

where

$$I_3^{(a)}(T) = T_{a_1 b_1 c_1} T_{a_1 b_1 c_2} T_{a_2 b_2 c_2} T_{a_3 b_2 c_3} T_{a_3 b_3 c_3} T_{a_2 b_3 c_1}, \quad (22)$$

and the other terms are again obtained by the color permutations ( $a \leftrightarrow b$ ) and ( $a \leftrightarrow c$ ).

Analogously, the  $I_3^{(a)}$  bubble can be split as

$$\exp \left[ -\frac{g_3 N^{3/2-1}}{6} I_3^{(a)}(T) \right] = \int [d\chi^{(3,a)}][d\bar{\chi}^{(3,a)}] \exp \left[ -N^{3/2} (\chi_{abc}^{(3,a)} \bar{\chi}_{abc}^{(3,a)} + i N^{-1/2} \sqrt{\frac{g_3}{6}} \hat{I}_P^{(b)}(T, \chi) + i N^{-1/2} \sqrt{\frac{g_3}{6}} \hat{I}_P^{(c)}(T, \bar{\chi})) \right]. \quad (23)$$

This provides a splitting of  $I_3(T)$  in two pillow interactions of different colors (see Fig. 8).

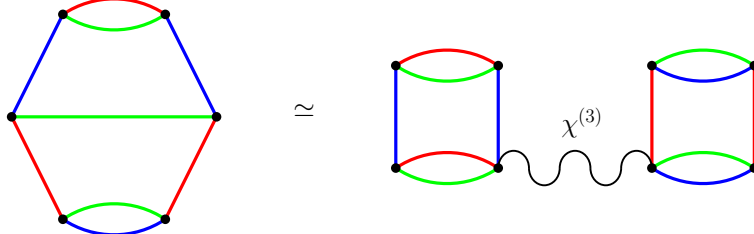


Figure 8: Intermediate field method for the  $I_3$  sextic interaction.

Note that in Fig. 8 a sum over color permutations is again implied.

Thus, the method we described here allows to reduce the order of the interactions in the model, from sextic to quartic, for all the interactions except  $I_2$  (not that interactions  $I_6, I_7, I_8$ , can be considered by definition of lower order, since the respective bubbles are not connected). This is a powerful tool to identify the behavior of the sextic bubbles in the large  $N$  limit since, the sextic large  $N$  limit can now be reconstructed from the known behavior of the quartic large  $N$  limit.

Note that the analysis above allows us to rewrite our general sextic model as a model with the wheel sextic interactions and a set of quartic interactions (the tetrahedron, the pillow) and the trace bubble, but with a non-trivial set of intermediate real or complex tensor fields ( $\chi^{(1)}, \chi^{(3)}, \chi^{(4)}$  and  $\chi^{(5)}$ ). We refer to the model with the sextic interactions and only one type of propagator as the *sextic representation* and the model with the quartic interactions and many propagators as the *quartic representation*.

## 4. No mixing of the wheel interaction

The first question one needs to address is whether or not one can find dominant fundamental graphs of the model which contain both the wheel interaction and quartic interactions. We prove in this section that no such mixing of interactions is allowed if the respective graph is dominant.

This holds for dominant fundamental graph  $\mathcal{G}$ . As usual in the tensor literature, we call a fundamental dominant graph a graph  $\omega(\mathcal{G}) = 0$  from which all the dominant graphs can be constructed *via* 2-points or 6-points insertions.

Note that, as a consequence of the analysis of the previous section, our model can now be studied as a model with a reduced set of interactions, namely the wheel, the tetrahedron, the pillow and the trace (Fig. 9).

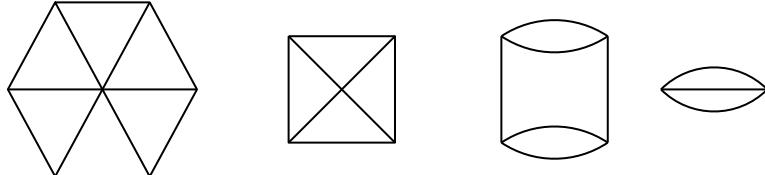


Figure 9: The reduced set of interactions that builds the sextic invariants.

In the case of 0–dimensional field theory, the computations of Feynman amplitudes is a pure combinatorial computation. Thus, we prove that the model with only one type of propagator instead of 5 types of propagators ( $T, \chi^{(1)}, \chi^{(3)}, \chi^{(4)}$  and  $\chi^{(5)}$ ) does not allow mixing between the wheel interaction and the tetrahedron interaction. This implies that the original model with 5 types of propagators does not allow this mixing either.

In order to simplify the notation, we thus choose to have a single type of field in our model. Later on, in order to identify explicitly the dominant graphs, we will come back to the original 5 field model.

The first step of the proof of the no mixing result is to further reduce the set of interactions by identifying two particular moves that preserve the degree. As already noticed in [29], the pillow interaction can be represented by two tetrahedric bubbles. Indeed, one can directly prove that the move defined in Fig. 10 doesn't change the degree.

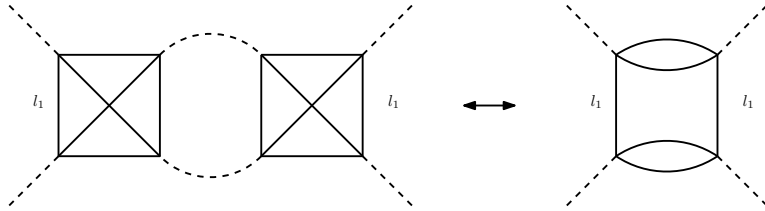


Figure 10: A replacement of a pillow by two tetrahedron.

The trace bubble also can be generated by tetrahedric bubbles, via the move defined in Fig. 11.

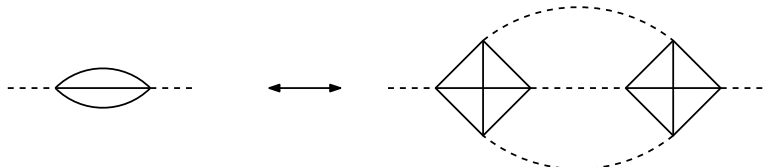


Figure 11: A replacement of a trace by two tetrahedron.

The model can therefore be further reduced to an even simpler model with only wheel and tetrahedron interactions that are allowed. We now exhibit the dominant graphs of this reduced model.

We consider a dominant Feynman graph  $\mathcal{G}$  containing both tetrahedric and wheel interaction, in the stranded representation. We first prove a bound on the number of faces of lengths 1, 2 and 3. We follow here [29] and consider the three Jackets  $\mathcal{J}_i$ ,  $i = 1, 2, 3$ , obtained by removing all the edges of color  $i$  from  $\mathcal{G}$ . One can prove that the jackets constructed in this way are ribbon graphs. Counting the faces of each such a ribbon jacket yields:

$$\sum_{i=1}^3 F(\mathcal{J}_i) = 2F(\mathcal{G}). \quad (24)$$

The number of faces of each jacket is given by

$$F(\mathcal{J}_i) + V(\mathcal{G}) - E(\mathcal{G}) = \sum_{n=1}^{N_i} 2 - 2h(\mathcal{J}_i^{(n)}), \quad (25)$$

where  $N_i$  is the number of connected component of  $\mathcal{J}_i$ ,  $h(\mathcal{J}_i^{(n)})$  is the non orientable genus of the  $n$ -th component of the  $i$ -th jacket and  $V(\mathcal{G})$  and  $E(\mathcal{G})$  denote the vertices, respectively the edges of the tensor Feynman graph  $\mathcal{G}$ . The tensor Feynman graph  $\mathcal{G}$  is dominant if all its ribbon jackets have genus 0 (and are thus planar).

We only consider tetrahedric and wheelic interactions such that

$$V(\mathcal{G}) = v_t + v_w \quad \text{and} \quad E(\mathcal{G}) = \frac{1}{2}(4v_t + 6v_w) = 2v_t + 3v_w, \quad (26)$$

where  $v_t$  and resp.  $v_w$  are the numbers of tetrahedric and resp. wheelic bubbles. We can thus express the total number of faces as

$$F(\mathcal{G}) = \frac{3}{2}v_t + 3v_w + (N_1 + N_2 + N_3). \quad (27)$$

Note that if  $\mathcal{G}$  is a dominant graph, then it contains an even number of tetrahedric bubbles, as in the  $O(N)^3$ -invariant quartic model.

The total number of faces can also be expressed as a sum of faces of length  $l$ :

$$F(\mathcal{G}) = \sum_{l \geq 1} F_l. \quad (28)$$

One then has

$$\sum_{l \geq 1} lF_l = 3E(\mathcal{G}) = 6v_t + 9v_w, \quad (29)$$

which further leads to

$$\sum_{l \geq 1} (4 - l)F_l = 4(N_1 + N_2 + N_3) + 3v_w. \quad (30)$$

This further rewrites as:

$$3F_1 + 2F_2 + F_3 = 4(N_1 + N_2 + N_3) + 3v_w + \sum_{l \geq 5} (l - 4)F_l. \quad (31)$$

Since each term on the RHS of the eq. (31) above is positive, one has the following bound:

$$3F_1 + 2F_2 + F_3 \geq 12 \geq 1 \quad (32)$$

Therefore a dominant graph has at least one face visiting one, two or three bubbles. Following the lines of [34], we use a weaker version of this bound, namely we use the fact that a dominant graph contains at least a cycle of length one, two or three. This comes from the fact a cycle is not necessarily a face in the bubble representation (see again Fig. 2).

Note that dominant graphs containing cycles visiting either only tetrahedric or only wheel bubbles have already been studied in [29, 34].

Let us first recall the results for these dominant graphs containing cycles visiting either only tetrahedric or only wheel bubble.

No dominant graph contains a cycle of length one visiting a tetrahedron (see again [29]). The only fundamental dominant graph containing a cycle visiting one wheel is the triple tadpole. Its form is given on Fig. 12 (see again [34]).

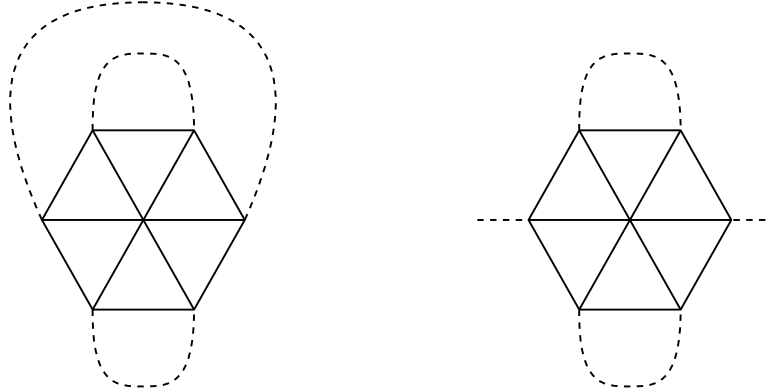


Figure 12: Fundamental dominant graphs containing a 1-cycle visiting a wheel bubble (left) and a corresponding tadpole insertion (right).

The 2-cycles can visit two tetrahedron ( $TT$ ), two wheels ( $WW$ ) or one tetrahedron and one wheel bubble ( $WT$ ). The dominant graphs containing a  $TT$  cycle or a  $WW$  cycle have again been found in [29, 34]. These are the melonic graphs (Fig. 13).

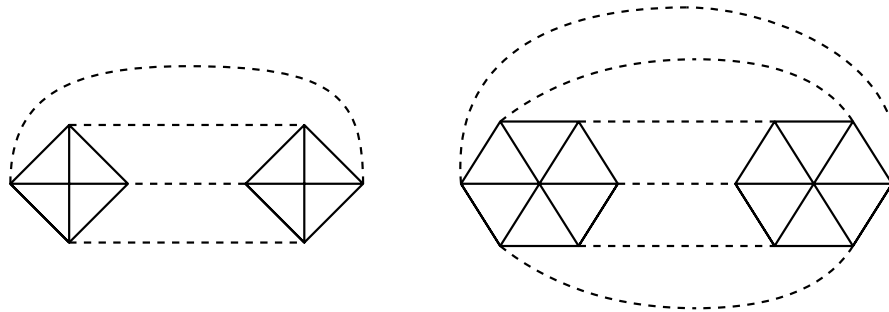


Figure 13: Fundamental dominant graphs containing a 2-cycle  $TT$  (left) and  $WW$  (right).

A dominant graph might also contain a 2-cycle visiting a tetrahedron and a wheel (a  $WT$  cycle). The general form of such graph is shown of Fig. 14 (left).

The  $TTT$  and resp. the  $WWW$  cycles have again been studied in [29] and resp. [34]. No fundamental dominant graph contains a  $TTT$  cycle. Analogously, no fundamental dominant graph contains a  $WWW$  cycle. However, a dominant graph containing a  $WWW$  cycle can only be constructed using the insertion of Fig. 12 (right) on a propagator of the graph of Fig. 13 (right). Note that this type of insertion cannot be done for the tetrahedric melon on the left of Fig. 13 since one needs to insert in this case a 2-point function containing (at least) two tetrahedric bubbles.

Let us now analyze the cases of mixed interaction:

- 2-cycles with  $WT$
- 3-cycles visiting mixed interactions ( $WTT$  and  $WWT$ ) can appear in dominant graphs.

We sum up all the possible cycles visiting mixed types of interactions that might appear in a dominant graph on Fig. 14.

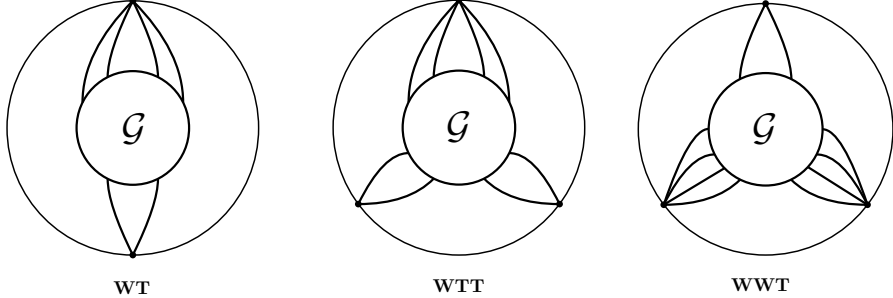


Figure 14: General shape of dominant graphs containing  $WT$ ,  $WTT$  or  $WWT$  cycles.

To identify the dominant graphs of the form given in Fig. 14, we follow a procedure introduced in [34], where this is used to identify the large  $N$  limit of a sextic model containing only prismatic and wheel interactions. The procedure is the following:

- Take one of the graphs in Fig. 14 and list all its possible inequivalent cycles (see subsection 2.2).
- For each inequivalent cycle, impose planarity for each ribbon jacket  $J_l$  (see Fig.15). In particular, remove the cycles that contain an odd number of twists.
- Planarity of each jacket imposes constraints on  $G$  from Fig.14. Only dominant graphs satisfy these constraints.

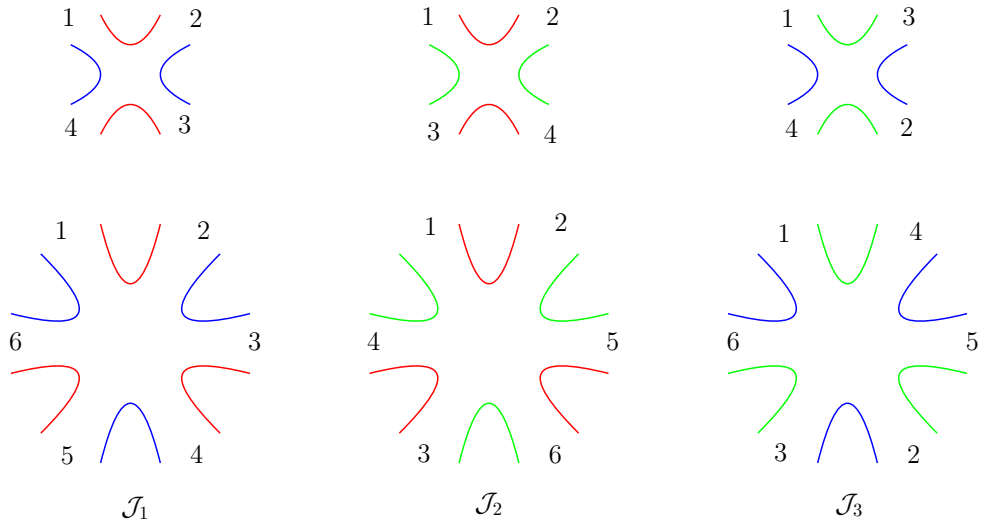


Figure 15: Jackets for the tetrahedron and the wheel bubble. The external bubble vertices are labeled.

**The WT cycle.** We find two inequivalent cycles with respect to color permutation cycles and bubble automorphisms:

- $\langle (1_W, 1_T), (2_W, 2_T) \rangle$
- $\langle (1_W, 1_T), (2_W, 4_T) \rangle$

These two cycles are not dominant because some of their ribbon jackets have an odd number of twists. For example, when we draw the first cycle in the  $\mathcal{J}_3$  jackets, we find that it has one twist (see Fig. 16). Therefore the corresponding graph containing this cycle in the stranded representation cannot be dominant.

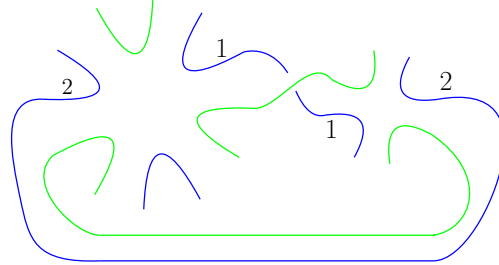


Figure 16: The  $\mathcal{J}_3$  jacket of a graph containing the  $\langle (1_L, 1_R), (2_R, 2_L) \rangle$  cycle.

This is also the case for the second cycle. We thus find that no dominant graph contains a *WT* cycle.

**The WTT cycle.** We find five inequivalent cycles visiting two wheels and a tetrahedron:

- $\langle (1_W, 1_T), (2_T, 1_{T'}), (\chi_{T'}, 2_W) \rangle$
- $\langle (1_W, 1_T), (4_T, 1_{T'}), (\zeta_{T'}, 2_W) \rangle$

where  $\chi = 2, 3, 4$  and  $\zeta = 2, 4$ . One has two allowed cycles:  $\langle (1_W, 1_T), (2_T, 1_{T'}), (2_{T'}, 2_W) \rangle$  and  $\langle (1_W, 1_T), (4_T, 1_{T'}), (4_{T'}, 2_W) \rangle$ . Planarity of each jacket constrains again the graphs containing these allowed cycles to have the generic shape shown on Fig. 17. This graph corresponds to a melonic graph built on two tetrahedron with a 2-point wheelic insertion on a propagator (or equivalently to a triple tadpole with a 2-point melonic insertion). The wheel insertion can be performed on every propagator of the melonic graph.

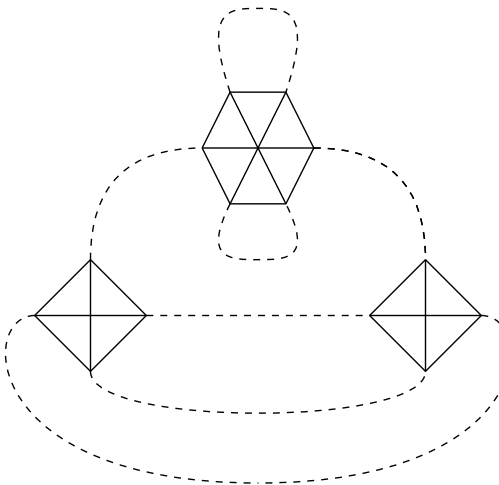


Figure 17: Dominant graph containing a *WTT* cycle.

Note that the allowed *WTT* cycles do not generate new fundamental structures, since graphs of the form given in Fig. 17 can be obtained from other fundamental graphs and insertions.

**The *WWT* cycle.** Graphs containing *WWT* cycles have the generic form given Fig. 14 (right).

One can prove that 17 inequivalent cycles can be built using two wheel and a tetrahedron bubble:

- $\langle (1_W, 1_{W'}), (2_{W'}, 1_T), (2_T, \alpha_W) \rangle$
- $\langle (1_W, 1_{W'}), (2_{W'}, 1_T), (3_T, \beta_W) \rangle$
- $\langle (1_W, 1_{W'}), (3_{W'}, 1_T), (\beta_T, \gamma_W) \rangle$

with  $\alpha \in \{2, 3, 4, 5, 6\}$ ,  $\beta \in \{2, 3, 4\}$  and  $\gamma \in \{2, 3, 5\}$ .

All these cycles have an odd number of twists in at least one of their ribbon jackets. This means that no dominant graph can contain a *WWT* cycle.

Let us now sum up the results obtained so far. We argued that every sextic bubble (except the wheel) can be decomposed in tetrahedric bubbles (using either the intermediate field method or the melonic moves of Fig. 10 and 11). We further proved that dominant graphs from this reduced model, built out of tetrahedron and wheel interactions, must contain at least one cycle of length 1, 2 or 3.

We find that the dominant graphs in this reduced model are the triple-tadpole graphs given in Fig. 12, the melon graphs given in Fig. 13 and the graph given in Fig. 17. However, the latter is not a fundamental dominant graph since it can be obtained from a 2–point wheel insertion (which conserves the degree) on a fundamental melon. This allows us to conclude that there are no fundamental dominant graphs containing both the wheel and the tetrahedron interaction. As a consequence, we have thus proved in this section, that there are no fundamental dominant graph that contains both the wheel and another sextic bubble.

## 5. Identification of the dominant graphs of the general model

For each bubble  $\mathcal{B}$ , we list the fundamental dominant graphs and the allowed insertions that conserve the degree. We then explicitly identify dominant graphs where several types of sextic bubbles, except the wheel one, can appear within the same graph.

### 5.1. The prismatic interaction

The large  $N$  limit of the prismatic bubble was studied in [23] with an intermediate field method. The only dominant fundamental graph is the graph of Fig. 18, where both the tetrahedric and prismatic representations are given. Note that, in the prismatic representation this fundamental dominant graph is a triple tadpole.

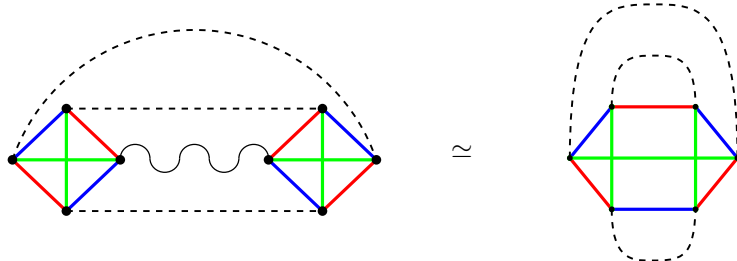


Figure 18: Dominant graph in the tetrahedric (left) and prismatic representation (right).

Following [28], and using the quartic representation, one can perform two kinds of insertions which conserve the degree of the graph:

1. a melonic insertion on the  $T_{abc}$  propagator and
2. a melonic insertion on the  $\chi_{abc}^{(1)}$  propagator (see Fig. 19).

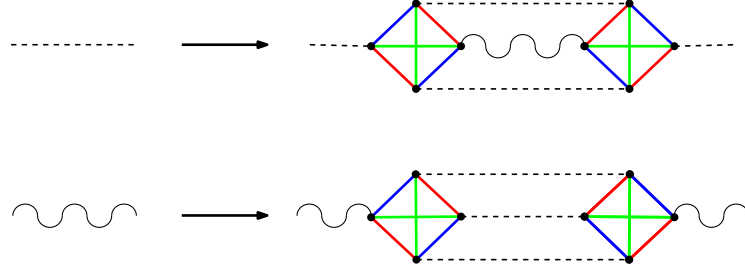


Figure 19: Melonic insertions on the  $T_{abc}$  and the  $\chi_{abc}^{(1)}$  propagator.

Using now the prismatic representations, two types of insertions are allowed:

1. The melonic insertions on  $T_{abc}$  propagator of Fig. 19 translates as a double tadpole insertion shown in Fig. 20. Note that the two double tadpoles of Fig. 20 are not equivalent from the point of view of index contractions.
2. The melonic insertion on the  $\chi_{abc}^{(1)}$  propagator of Fig. 19 translates as an insertion at the level of the  $I_1$  bubble (see Fig. 21).

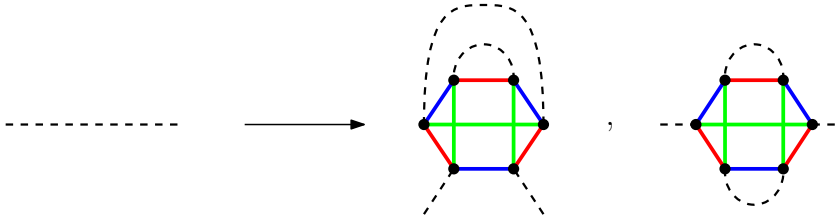


Figure 20: Double tadpole insertion on the  $T_{abc}$  propagator.

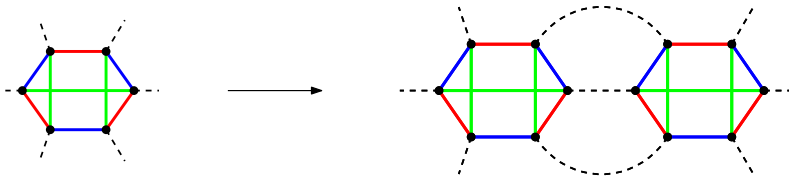


Figure 21: Melonic insertion in the  $I_1$  bubble in the prismatic representation.

Note that the insertion in Fig. 21 is a vertex insertion, as already explained in [28].

## 5.2. The wheel interaction

The fundamental dominant graphs containing only wheel interactions have been found in section 4. We list them in Fig. 22.

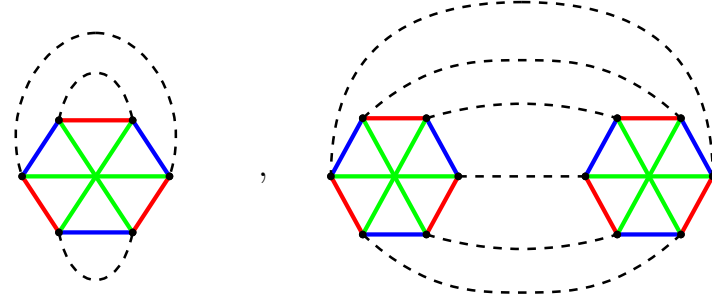


Figure 22: Fundamental dominant graphs built on  $g_2$ . The triple tadpole (left) and the melon (right).

The 2-point insertions conserving the degree are shown on Fig. 23. These insertions are obtained by cutting an edge in the fundamental dominant graphs.

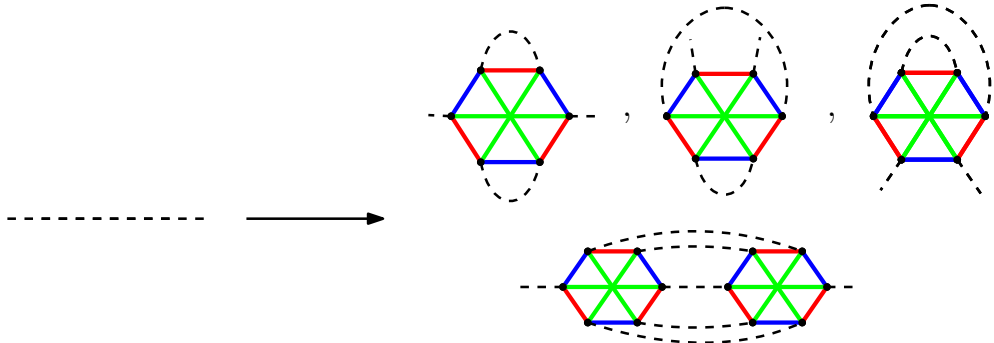


Figure 23: 2-point insertion for the  $I_2$  interaction.

### 5.3. The $I_3$ and $I_4$ interaction

Recall that the  $I_3$  interaction can be split, using the intermediate field method, in two pillow interactions of different colors (see Fig. 8 above). The only dominant graph one can construct using only this interaction is given, in the quartic and sextic representation, in Fig. 24. Note that, once again, the dominant graph in the sextic representation is a triple tadpole.

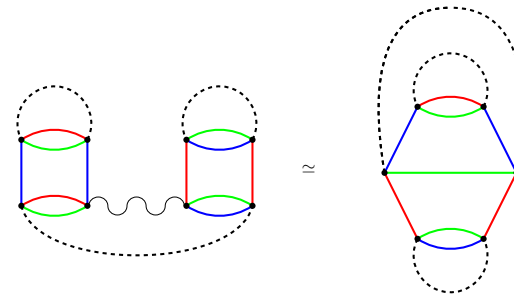


Figure 24: Fundamental graph from  $I_3$  in the quartic (left) and sextic representation (right).

The insertions conserving the degree are, once again, obtained by cutting one edge in the dominant graphs. This can be done in three distinct ways (Fig. 25).

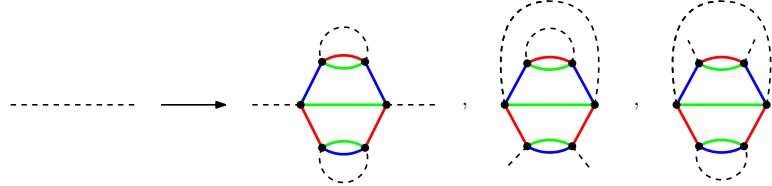


Figure 25: 2–points insertions for the  $I_3$  interaction.

As above, recall that the  $I_4(T)$  interaction is split, using the intermediate field method, in two pillow interactions which are of the same color (see Fig. 6). The only dominant graph one can construct using only this interaction is, once again, the triple tadpole. We give this dominant graph in the quartic and sextic representation, in Fig. 26.

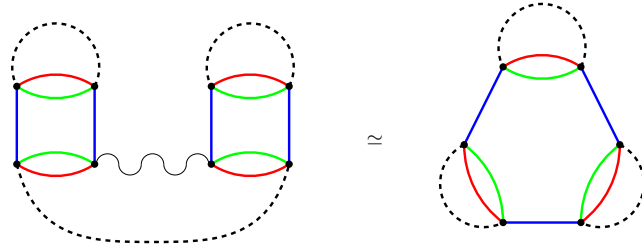


Figure 26: Dominant graph from  $I_4$  in the quartic (left) and sextic representation (right).

The insertions conserving the degree is obtained by cutting an edge in the dominant graph. Only one insertion is allowed (Fig. 27).



Figure 27: 2–point insertions for the  $I_4(T)$  interaction.

#### 5.4. The $I_5$ and $I_6$ interaction

As above, recall that the  $I_5(T)$  interaction is split, using the intermediate field method, in a pillow and a tetrahedron interactions - see 7. The only dominant graph one can now construct using only this interaction is given, in the quartic and sextic representation, in Fig. 28.

Let us emphasize here that the type of dominant graph of Fig. 28 is to our knowledge, new with respect to the types of dominant graphs known so far for various tensor models.

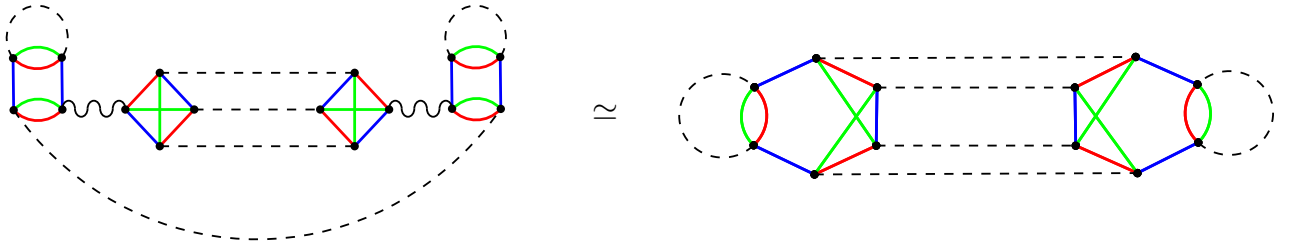


Figure 28: Dominant graph formed with  $I_5(T)$ .

The insertions conserving the degree are obtained again by cutting an edge in the dominant graph. Two insertions are allowed, see Fig. 29.

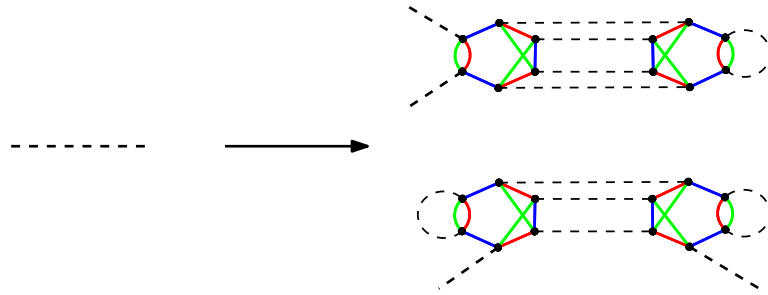


Figure 29: Dominant 2-point insertions for the  $I_5(T)$  interaction.

Let us now analyze the  $I_6$  interaction. Recall that this interaction is a disconnected one built on a tetrahedron and a trace. The dominant graphs are thus the melon graph (formed with two  $g_6$  bubbles) of Fig. 30).

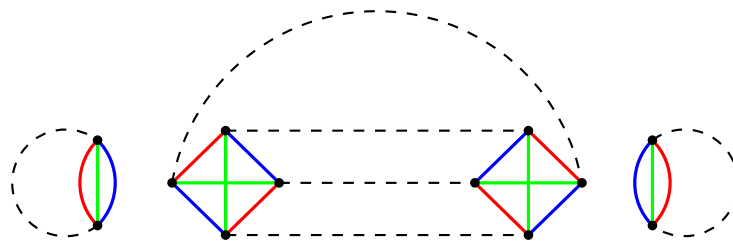


Figure 30: Dominant graph formed with  $I_6(T)$ .

The 2-point insertions conserving the degree are again obtained by cutting an edge in the dominant graph, see Fig. 31.

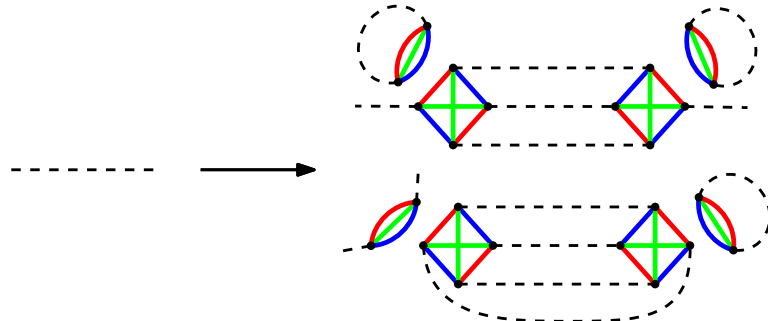


Figure 31: 2-point insertions for the  $I_6$  interaction.

### 5.5. The $I_7$ and the $I_8$ bubbles

The  $I_7$  and  $I_8$  bubbles are again disconnected and their large  $N$  behavior is known. The fundamental dominant graphs are the triple tadpoles of Fig. 32.

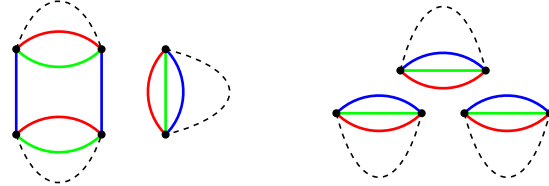


Figure 32: Dominant fundamental graphs for the  $I_7(T)$  interaction (left) and the  $I_8(T)$  interaction (right).

The 2-point insertions that conserve the degree are, once again, obtained by cutting an edge in any of the fundamental dominant graphs, see Fig. 33.

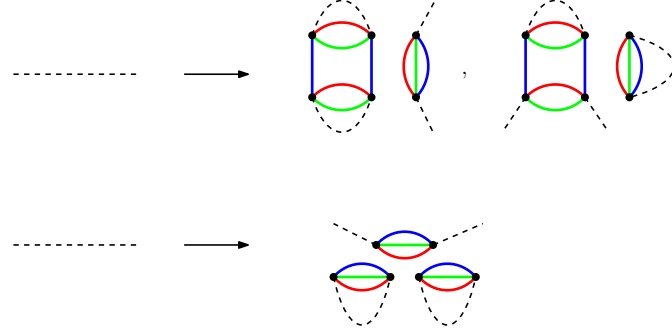


Figure 33: 2-point insertions built  $I_7(T)$  (top) and  $I_8(T)$  (bottom).

## 5.6. Dominant graph containing several types of sextic interactions

Note that, one can have several sextic interactions within the same fundamental dominant graph, except for the wheel one. Let us emphasize that in the case of the  $U(N)^3$  invariant model studied in [33] one cannot have dominant graphs containing several sextic interactions. However, this becomes possible for the  $O(N)^3$  model studied here, as a consequence of the additional  $I_1$ ,  $I_5$  and  $I_6$  interactions.

Using the intermediate field method and the large  $N$  behavior for quartic interactions, we find four new fundamental dominant graphs containing mixed bubbles which we show on Fig. 34. We denote these diagrams by  $\mathcal{G}_1$  to  $\mathcal{G}_4$ . Using eq. (11) we show that their degree is vanishing:

$$\begin{aligned}
 \omega(\mathcal{G}_1) &= 3 + \frac{7}{2} + \frac{9}{2} - 11 = 0, \\
 \omega(\mathcal{G}_2) &= 3 + 2 \times \frac{7}{2} + 3 - 13 = 0, \\
 \omega(\mathcal{G}_3) &= 3 + 2 \times \frac{9}{2} + 3 - 15 = 0, \\
 \omega(\mathcal{G}_4) &= 3 + \frac{7}{2} + \frac{9}{2} + 3 - 14 = 0.
 \end{aligned} \tag{33}$$

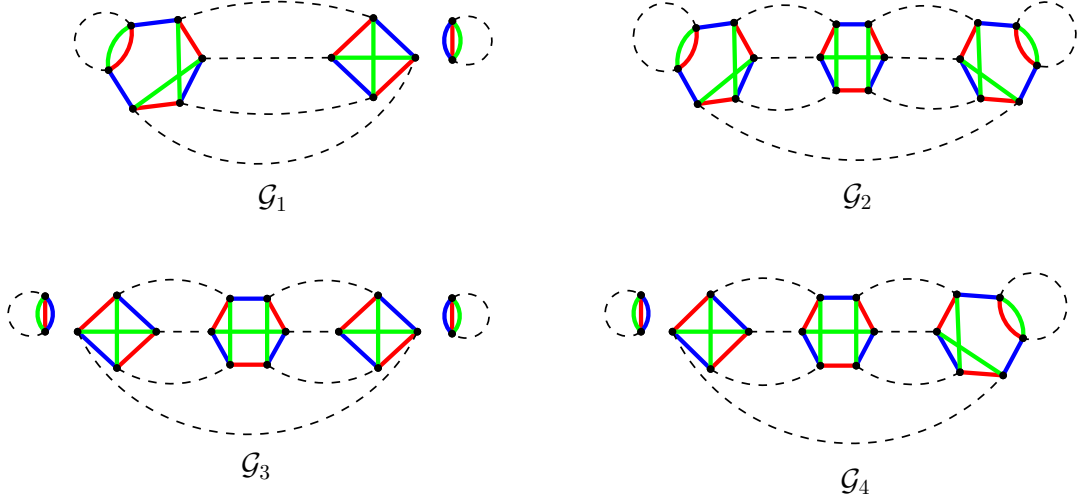


Figure 34: Fundamental dominant graphs with mixed interactions.

Let us note that, one can use any of the new types of dominant graph of Fig. 34 to generate a series of non-fundamental dominant graphs, which are obtained, as usual, *via* 2-point insertions which preserve the degree. The pattern to be inserted is obtained, as usually, by cutting an edge in any of these fundamental vacuum graphs.

### 5.7. Summary of the large $N$ limit results

We list here all the possible fundamental dominant graphs of our general sextic model (5). This list of Feynman graphs is given in Fig. 35, where we indicate which interactions are allowed in each case.

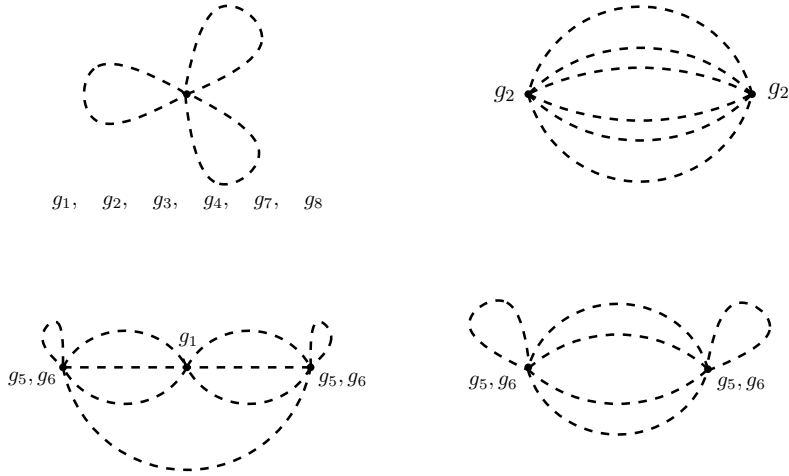


Figure 35: Dominant fundamental graphs for the  $O(N)^3$ -invariant sextic model.

A general, non-fundamental, dominant graph is obtained by taking one of the fundamental vacuum graph from Fig. 35 and performing repeated insertions on some propagator and in the prismatic bubble. The allowed propagator-insertions are listed on Fig. 36 and the melonic insertion in the prismatic bubble is shown on Fig. 21.

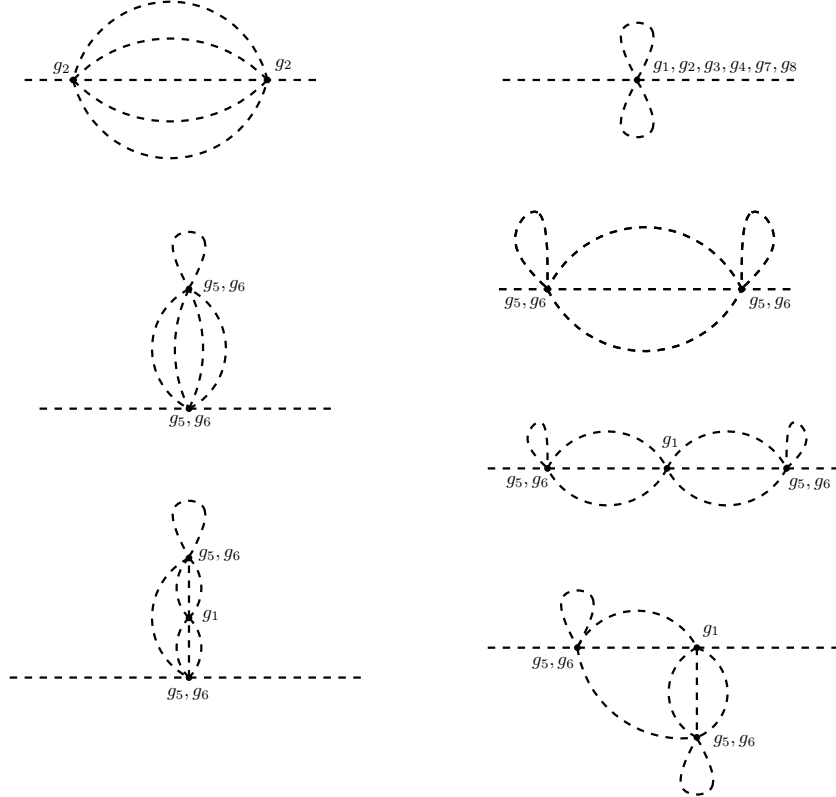


Figure 36: Possible degree-preserving insertions on the propagator.

## 6. Conclusion

We implemented the large- $N$  limit mechanism for the  $O(N)^3$ -invariant sextic tensor model, taking into consideration all 8 invariant bubbles with optimal scalings.

Using the intermediate field method and melonic moves, we reduced the initial set of sextic bubbles to a minimal set of building blocks, consisting only of the wheel and the tetrahedron bubbles:

$$\{I_b(T)\}_{b=1}^8 \xrightarrow{\text{intermediate field}} \{I_2(T), I_t(T, \chi), I_p(T, \chi)\} \xrightarrow{\text{Melonic moves}} \{I_2(T), I_t(T, \chi)\}. \quad (34)$$

This reduced model allowed us to identify dominant graphs. Planarity constraints on ribbon jackets ruled out fundamental dominant graphs mixing the wheel with other sextic interactions. Using the known results for the quartic case, we reconstructed the sextic representation, explicitly identifying the dominant graphs and the degree conserving moves.

The resulting large- $N$  structure is much richer than in previously studied tensor models. In particular, mixed-bubble structures and melonic insertions in the prismatic vertex generate complex dominant diagrams, as illustrated in Fig. 37, and even infinite families of dominant graphs, see Fig. 38.

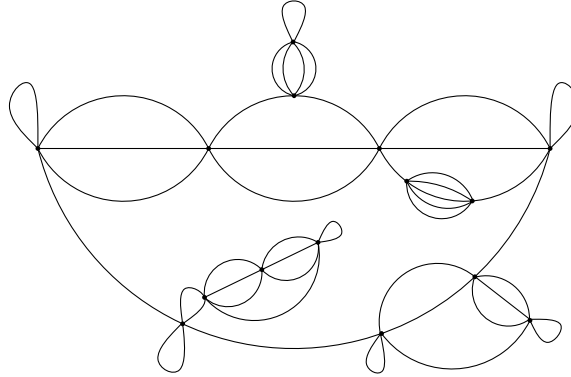


Figure 37: Example of a high-order dominant graph. Mixed structures together with melonic insertions in the prismatic bubble generate intricate diagrams.

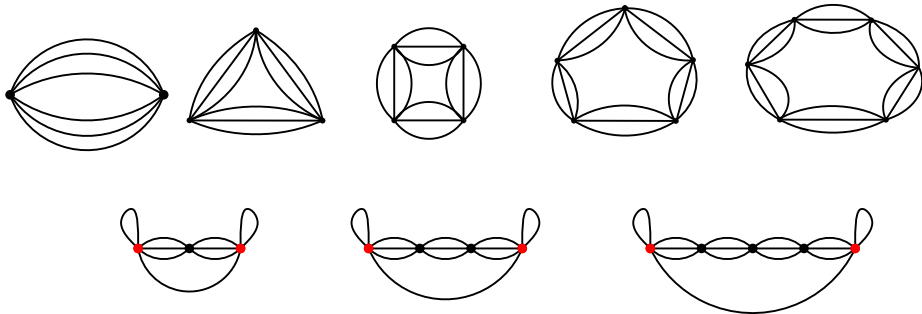


Figure 38: First graphs in the two infinite families generated by recursive melonic insertions in the prismatic vertex. Edges denote the full 2-point function. Black dots are prismatic vertices; red dots are  $g_5$  or  $g_6$ .

Let us end this paper by listing several natural perspectives for future work:

- Can the method developed here be generalized to higher order interactions, to identify the minimal set of bubbles from which all higher-order interactions can be reconstructed?
- The prismatic vertex insertion generates infinite sequences of dominant Feynman graphs. Is there a general criterion which determines which tensor interactions leads to such infinite families? Moreover, one can wonder whether or not higher-order bubbles can play a similar role?
- While melonic Feynman integrals are well understood, the present model produces more intricate dominant graphs. Can the corresponding Feynman integrals be classified and computed systematically, potentially enabling progress on solving Schwinger–Dyson equations beyond the melonic sector?
- If one considers the model studied here as a tensorial field theoretical model, non-trivial renormalization flow questions arise. This constitutes the topic of a companion paper [48].

## A. Optimal scalings

The optimal scaling for interaction  $b$  is  $\rho(b) = \frac{1}{2} \sum_{l=1}^3 \delta_l^{(b)}$ , where  $\delta_l^{(b)} = |J_l^{(b)}| - 1$ , with  $|J_l^{(b)}|$  the number of connected components of the  $l$ -th jacket of the  $b$ -th bubble.

We show the three jackets for each bubble and scalings computation on Fig. 39.

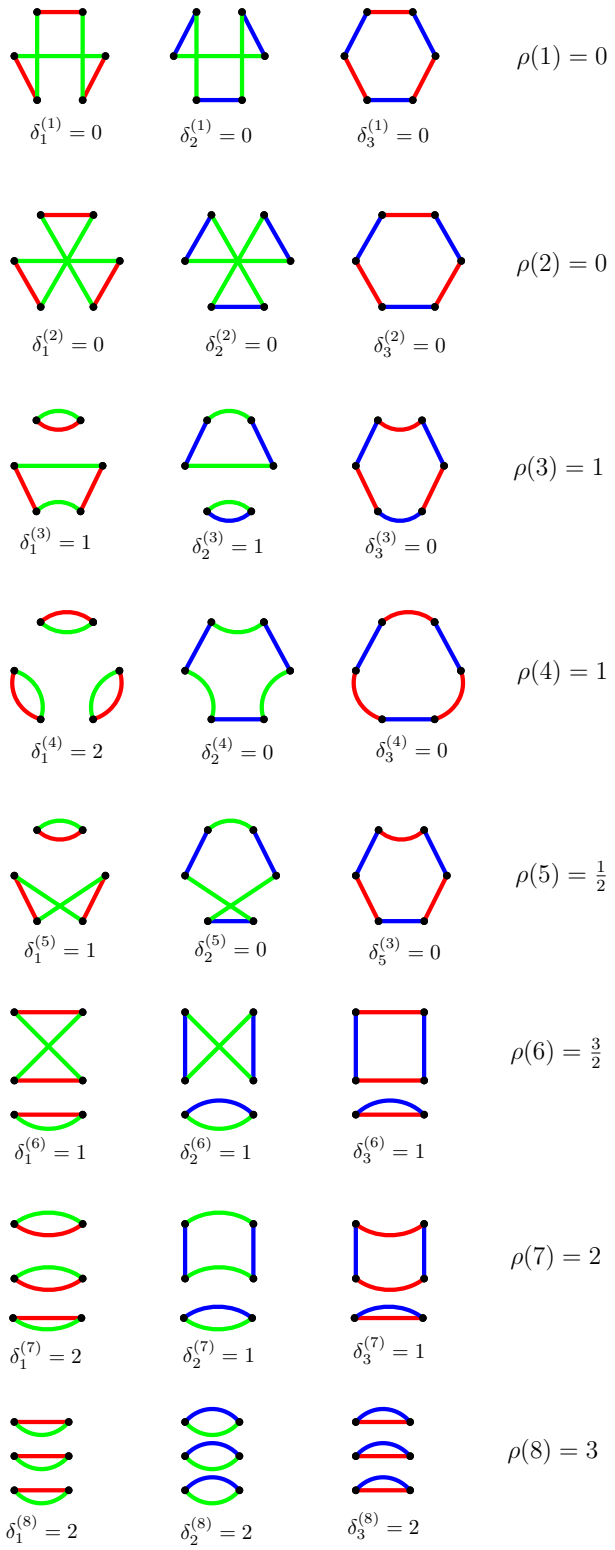


Figure 39: Optimal scalings computation

## References

- [1] M. Moshe and J. Zinn-Justin, “Quantum field theory in the large  $N$  limit: a review,” *Physics Reports*, vol. 385, p. 69–228, Oct. 2003.
- [2] G. Eyal, M. Moshe, S. Nishigaki, and J. Zinn-Justin, “The  $O(N)$  vector model in the large  $N$  limit revisited: multicritical points and double scaling limit,” *Nuclear Physics B*, vol. 470, p. 369–395, July 1996.
- [3] G. Hooft, “A planar diagram theory for strong interactions,” *Nuclear Physics B*, vol. 72, no. 3, pp. 461–473, 1974.
- [4] E. Brezin, C. Itzykson, G. Parisi, and J. B. Zuber, “Planar Diagrams,” *Commun. Math. Phys.*, vol. 59, p. 35, 1978.
- [5] V. Kazakov, I. Kostov, and A. Migdal, “Critical properties of randomly triangulated planar random surfaces,” *Physics Letters B*, vol. 157, no. 4, pp. 295–300, 1985.
- [6] F. David, “Planar diagrams, two-dimensional lattice gravity and surface models,” *Nuclear Physics B*, vol. 257, pp. 45–58, 1985.
- [7] M. Marino, “Les Houches lectures on matrix models and topological strings,” 2004. arXiv:hep-th/0410165.
- [8] B. Eynard, T. Kimura, and S. Ribault, “Random matrices,” 2015. arXiv:1510.04430 [math-ph].
- [9] P. Ginsparg, “Matrix models of 2d gravity.” Presented at the Trieste Summer School, Trieste (Italy), 22-25 Jul. 1991, Jan. 1991.
- [10] P. H. Ginsparg and G. W. Moore, “Lectures on 2D gravity and 2D string theory,” in *Theoretical Advanced Study Institute (TASI 92): From Black Holes and Strings to Particles*, pp. 277–469, 10 1993.
- [11] P. Di Francesco, “2D Quantum Gravity, Matrix Models and Graph Combinatorics,” *arXiv e-prints*, pp. math-ph/0406013, June 2004.
- [12] N. Sasakura, “Tensor Model for Gravity and Orientability of Manifold,” *Modern Physics Letters A - MOD PHYS LETT A*, vol. 6, pp. 2613–2623, Sept. 1991.
- [13] J. Ambjørn, B. Durhuus, and T. Jónsson, “Three-Dimensional Simplicial Quantum Gravity and Generalized Matrix Models,” *Modern Physics Letters A*, vol. 6, pp. 1133–1146, Jan. 1991. ADS Bibcode: 1991MPLA....6.1133A.
- [14] R. G. Gurău, *Random Tensors*. Oxford University Press, 10 2016.
- [15] A. Tanasa, *Combinatorial Physics: Combinatorics, Quantum Field Theory, and Quantum Gravity Models*. Oxford University Press, 04 2021.
- [16] R. Gurau, “The  $1/N$  expansion of colored tensor models,” *Annales Henri Poincaré*, vol. 12, p. 829–847, Mar. 2011.
- [17] S. Sachdev and J. Ye, “Gapless spin-fluid ground state in a random quantum Heisenberg magnet,” *Physical Review Letters*, vol. 70, p. 3339–3342, May 1993.
- [18] A. Kitaev, “A simple model of quantum holography (part 1).” Kavli Institute for Theoretical Physics Program: Entanglement in Strongly-Correlated Quantum Matter, Apr. 2015.

- [19] E. Witten, “An syk-like model without disorder,” *J. Phys. A*, vol. 52, no. 47, p. 474002, 2019.
- [20] R. Gurau, “The complete  $1/N$  expansion of a SYK-like tensor model,” *Nuclear Physics B*, vol. 916, pp. 386–401, 2017.
- [21] C. Krishnan, S. Sanyal, and P. N. B. Subramanian, “Quantum chaos and holographic tensor models,” *Journal of High Energy Physics*, vol. 2017, Mar. 2017.
- [22] S. Giombi, I. R. Klebanov, and G. Tarnopolsky, “Bosonic tensor models at large  $N$  and small  $\varepsilon$ ,” *Physical Review D*, vol. 96, Nov. 2017.
- [23] S. Giombi, I. R. Klebanov, F. Popov, S. Prakash, and G. Tarnopolsky, “Prismatic large  $N$  models for bosonic tensors,” *Physical Review D*, vol. 98, Nov. 2018.
- [24] D. Benedetti, R. Gurau, and S. Harribey, “Line of fixed points in a bosonic tensor model,” *Journal of High Energy Physics*, vol. 2019, June 2019.
- [25] C. Jepsen and Y. Oz, “RG flows and fixed points of  $O(N)^r$  models,” *JHEP*, vol. 02, p. 035, 2024.
- [26] R. Gurau, “The complete  $1/N$  expansion of colored tensor models in arbitrary dimension,” *Annales Henri Poincaré*, vol. 13, pp. 399–423, Apr. 2012. arXiv:1102.5759 [gr-qc].
- [27] V. Bonzom, V. Nador, and A. Tanasa, “Double scaling limit for the  $O(N)^3$ -invariant tensor model,” *Journal of Physics A: Mathematical and Theoretical*, vol. 55, p. 135201, Mar. 2022.
- [28] T. Krajewski, T. Muller, and A. Tanasa, “Double scaling limit of the prismatic tensor model,” *Journal of Physics A: Mathematical and Theoretical*, vol. 56, p. 235401, May 2023.
- [29] S. Carrozza and A. Tanasa, “ $O(N)$  random tensor models,” *Letters in Mathematical Physics*, vol. 106, p. 1531–1559, Aug. 2016.
- [30] V. Bonzom, L. Lionni, and V. Rivasseau, “Colored triangulations of arbitrary dimensions are stuffed walsh maps,” *The Electronic Journal of Combinatorics*, vol. 24, 2017.
- [31] L. Lionni and J. Thürigen, “Multi-critical behaviour of 4-dimensional tensor models up to order 6,” *Nuclear Physics B*, vol. 941, pp. 600–635, 2019.
- [32] L. Lionni, *Colored Discrete Spaces: Higher Dimensional Combinatorial Maps and Quantum Gravity*. Springer International Publishing, 2018.
- [33] D. Benedetti, N. Delporte, S. Harribey, and R. Sinha, “Sextic tensor field theories in rank 3 and 5,” *Journal of High Energy Physics*, vol. 2020, June 2020.
- [34] S. Prakash and R. Sinha, “Melonic dominance in subchromatic sextic tensor models,” *Physical Review D*, vol. 101, June 2020.
- [35] L. Fraser-Taliente and J. Wheater, “Melonic limits of the quartic Yukawa model and general features of melonic CFTs,” *JHEP*, vol. 01, p. 187, 2025.
- [36] R. L. Stratonovich, “On a Method of Calculating Quantum Distribution Functions,” *Soviet Physics Doklady*, vol. 2, p. 416, July 1957.
- [37] J. Hubbard, “Calculation of partition functions,” *Phys. Rev. Lett.*, vol. 3, pp. 77–78, Jul 1959.
- [38] V. Rivasseau and Z. Wang, “How to resum feynman graphs,” *Annales Henri Poincaré*, vol. 15, p. 2069–2083, Dec. 2013.

- [39] L. Lionni and V. Rivasseau, “Intermediate Field Representation for Positive Matrix and Tensor Interactions,” *Annales Henri Poincare*, vol. 20, no. 10, pp. 3265–3311, 2019.
- [40] S. Harribey, “Sextic tensor model in rank 3 at next-to-leading order,” *Journal of High Energy Physics*, vol. 2022, p. 37, Oct. 2022.
- [41] S. Carrozza and V. Pozsgay, “SYK-like tensor quantum mechanics with  $Sp(N)$  symmetry,” *Nucl. Phys. B*, vol. 941, pp. 28–52, 2019.
- [42] R. L. Mkrtchyan, “The equivalence of  $Sp(2N)$  and  $SO(-2N)$  gauge theories,” *Physics Letters B*, vol. 105, no. 2, pp. 174–176, 1981.
- [43] M. Mulase and A. Waldron, “Duality of orthogonal and symplectic matrix integrals and quaternionic feynman graphs,” *Communications in Mathematical Physics*, vol. 240, pp. 553–586, Sept. 2003. arXiv:math-ph/0206011.
- [44] H. Keppler and T. Muller, “Duality of orthogonal and symplectic random tensor models: general invariants,” *Lett. Math. Phys.*, vol. 113, no. 4, p. 83, 2023.
- [45] H. Keppler and T. Muller, “Duality of orthogonal and symplectic random tensor models: general invariants,” *Letters in Mathematical Physics*, vol. 113, no. 4, 2023.
- [46] H. Keppler, T. Krajewski, T. Muller, and A. Tanasa, “Duality of  $O(N)$  and  $Sp(N)$  random tensor models: tensors with symmetries,” *Journal of Physics A: Mathematical and Theoretical*, vol. 56, p. 495206, Nov. 2023.
- [47] T. Muller, *Study of combinatorial objects in higher dimensions*. PhD thesis, Université de Bordeaux, 2025.
- [48] G. Bardy, T. Krajewski, T. Muller, and A. Tanasa, “Renormalization group flow of the  $O(N)^3$ –invariant general sextic tensor model,” *to be submitted*, 2025.